Songklanakarin J. Sci. Technol.
42 (4), 802-810, Jul. - Aug. 2020

http://www.sjst.psu.ac.th

Original Article

In silico screening of chalcones against Epstein-Barr virus nuclear antigen 1 protein

Nitchakan Darai[1, 2], Panupong Mahalapbutr[2], Kanyani Sangpheak[1, 2], Chompoonut Rungnim[3], Peter Wolschann[4, 5], Nawee Kungwan[6, 7], and Thanyada Rungrotmongkol[2, 8*]

[1] *Program in Biotechnology, Faculty of Science, Chulalongkorn University, Pathum Wan, Bangkok, 10330 Thailand*

[2] *Full Structural and Computational Biology Research Group, Department of Biochemistry, Faculty of Science, Chulalongkorn University, Pathum Wan, Bangkok, 10330 Thailand*

[3] *Full National Nanotechnology Center, National Science and Technology Development Agency, Khlong Luang, Pathum Thani, 12120 Thailand*

[4] *Department of Pharmaceutical Chemistry, University of Vienna, Spitalgasse, Vienna, 1090 Austria*

[5] *Institute of Theoretical Chemistry, University of Vienna, Spitalgasse, Vienna, 1090 Austria*

[6] *Department of Chemistry, Faculty of Science, Chiang Mai University, Mueang, Chiang Mai, 50200 Thailand*

[7] *Research Center on Chemistry for Development of Health Promoting Products from Northern Resources, Chiang Mai University, Mueang, Chiang Mai, 50200 Thailand*

[8] *Graduate Programs in Bioinformatics and Computational Biology, Faculty of Science, Chulalongkorn University, Pathum Wan, Bangkok, 10330 Thailand*

Received: 9 November 2018; Revised: 10 April 2019; Accepted: 18 April 2019

Abstract

The Epstein-Barr nuclear antigen 1 (EBNA1) is a crucial protein expressed by the Epstein-Barr virus (EBV). The EBNA1 is necessary for the replication and transcriptional regulation of latent gene expression of the EBV. Therefore, it is connected with some diseases, especially malignancies. Previous studies have shown that chalcone potentially inhibited the EBV virus; therefore, in this study a series of chalcones were screened *in silico* toward EBNA1 by the use molecular docking and molecular dynamics simulation. The results suggested that chalcone 3a displayed significantly greater binding affinity than the reported anti-EBV agents. The EBNA1 residues K477, I481, N519, K586, and T590 contributed mainly for the chalcone 3a binding at the recognition helix site. Altogether, this chalcone might serve as a lead compound acting against EBNA1.

Keywords: chalcone, Epstein-Barr virus nuclear antigen 1 protein, natural products, molecular docking, molecular dynamics simulation

*Corresponding author
Email address: t.rungrotmongkol@gmail.com; thanyada.r@chula.ac.th

1. Introduction

The Epstein-Barr virus (EBV) is a member of the herpesvirus family that was discovered by Epstein, Achong, and Barr from Burkitt's lymphoma tissue (Cohen, 2000). EBV infects around 90% of humans and persists for the entire lifetime. Viral spread commonly occurs through saliva, by sexual contact, and by blood and organ transplantations. EBV is spread widely around the world and is connected with an increasing number of autoimmune diseases, including Burkitt's lymphoma, Hodgkin's lymphoma (Vrzalikova, Sunmonu, Reynolds, & Murray, 2018), and gastric (Boudreault, Armero, Scott, Perreault, & Bisaillon, 2019) and nasopharyngeal carcinomas (Middeldorp, 2015). During latent infection, EBV expresses some viral gene products for proliferation and promotes host cell survival (Li *et al.*, 2010).

The Epstein-Barr nuclear antigen 1 (EBNA1) protein is encoded by the EBV and it is the key molecular target due to its essential role in the preservation of EBV episomes in the dividing host cells. EBNA1 is a protein dimer that binds in a sequence-specific way to DNA, in particular to the 18 base-pair (bp) palindromic recognition site present at the origin plasmid replication (oriP) of the EBV (Leight & Sugden, 2000). The oriP of the EBV carries the family of repeats (FR) element and the dyad symmetry (DS) element. The FR element is comprised of an array of 30 bp units, in which each unit has one EBNA1 binding site. EBNA1 bound with FR conducts tethering of the oriP containing plasmid to the chromosome and causes non-random segregation of EBV episomes in proliferating cells (Yasuda *et al.*, 2011). The DS element consists of four EBNA1 binding sites and appears to function as a replicator (Schepers *et al.*, 2001). The two crystal structures of EBNA1 have been solved by high resolution X-ray crystallography. 1VHI is the structure of EBNA1 without DNA binding, while 1B3T is EBNA1 protein co-crystallized with the palindromic DNA recognition sequence (Bochkarev, Mincione, Coratti, Fabrizi, & Battistuzzi, 1998) (Figure 1).

Chalcones are plant-derived polyphenolic compounds that are interesting because of their remarkable pharmacological activities (Evranos & Ertan, 2011) and their anti-inflammatory, antibacterial, antifungal, antiviral, and antineoplastic properties (Bernini, Mincione, Coratti, Fabrizi, & Battistuzzi, 2004; Choudhary & Juyal, 2011). Structurally, chalcones have two aromatic rings that are connected by a carbon-carbon double bond and a carbonyl carbon atom which is typical for open chain flavonoids. Results of *in vitro* EBV early antigen induction and neuron-derived orphan receptor-1 inhibition tests concluded that 4-hydroxyderricin, which is the chalcone compound extracted from the exudate of Ashitaba stems, could potentially inhibit EBV (Akihisa *et al.*, 2003). *In silico* screening (Li *et al.*, 2010) using a publically available molecular database containing 90,000 compounds toward EBNA1 leads to a series of substances with half maximal inhibitory concentration (IC_{50}) values in the 20 micromolar range against EBNA1. Gianti, Messick, Lieberman, and Zauhar (2016) performed a computational identification and a structural characterization of EBNA1 binding pockets and validated docking predictions of a set of substances tested *in vitro* for EBNA1 inhibition (PubChem AID-2381). They reported the drug's ability to bind pockets by applying induced fit docking as well as molecular dynamics (MD) simulations together with binding affinity predictions based on the molecular mechanics/generalized Born surface area (MM/GBSA) technique.

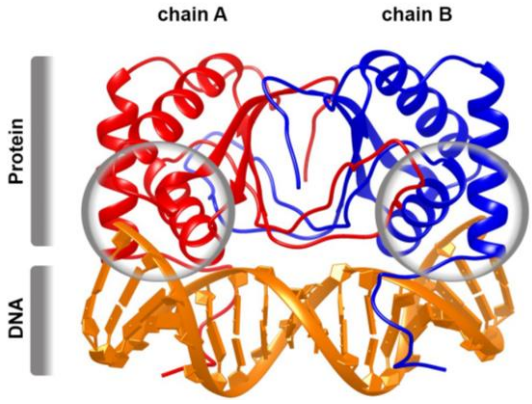

Figure 1. Crystal structure of EBNA1 (PDB entry code: 1B3T), in which the chains A, B, and DNA are shaded by red, blue, and orange, respectively. The recognition helix (RH) site is represented by the grey sphere.

In the present study, the 47 designed chalcone derivatives (Figure 2) were screened *in silico* toward the recognition helix (RH) site (Figure 1) in order to find a new attractive candidate against the EBNA1 protein. Subsequently, the all-atom molecular dynamics simulations were applied on the focused chalcones in complex with EBNA1 in order to investigate structural and dynamical properties and the ligand-target interactions. Moreover, the binding affinities of the complexes were estimated using MM/GBSA calculations.

2. Materials and Methods

2.1 System setup and molecular docking

The crystal structure of EBNA1 nuclear protein (PDB entry code: 1B3T) is given in the Protein Data Bank (Bochkarev, Bochkareva, Frappier, & Edwards, 1998). The protonation state of all charged side chains of the EBNA1 protein was assigned at pH 7.0 by the PROPKA 3.0 server (Olsson, Sondergaard, Rostkowski, & Jensen, 2011). All structural parameters of the 47 chalcone derivatives were created by the Gaussian09 program (Frisch *et al.*, 2009) using the HF/6-31(d) level of theory. Subsequently, each complex with EBNA1 was built by molecular docking into the RH site with 100 docking runs applying the CDOCKER module (Wu, Robertson, Brooks, & Vieth, 2003) of the Accelrys Discovery Studio 3 (Accelrys Inc., San Diego, CA, USA) and iGEMDOCK program using the standard docking procedures (Jinn-Moon, & Chun-Chen, 2004). Subsequently, the best docked complexes were further studied by the MD simulations in aqueous solutions using the AMBER16 software package.

2.2 Molecular dynamics simulation

According to standard procedures (Nutho *et al.*, 2014; Sangpheak, Khuntawee, Wolschann, Pongsawasdi, & Rungrotmongkol, 2014) the missing hydrogen atoms of the

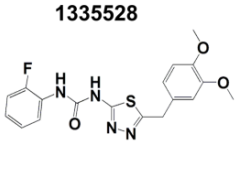

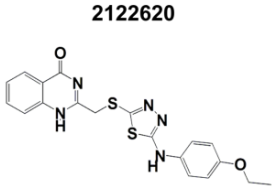

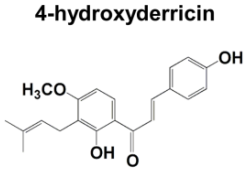

Group 1

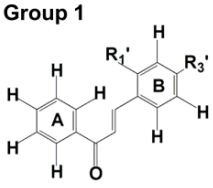

	R1'	R3'
1a	H	OCH_3
1b	H	OH
1c	OH	H

Group 2

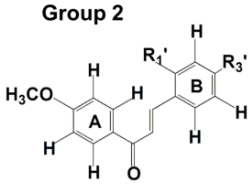

	R1'	R3'
2a	OH	H
2b	H	OH
2c	H	OCH_3
2d	H	$C(CH_3)_3$

Group 3

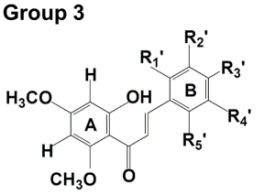

	R1'	R2'	R3'	R4'	R5'
3a	OCH_3	H	OCH_3	H	H
3b	OCH_3	H	H	OCH_3	H
3c	OCH_3	H	OCH_3	H	OCH_3
3d	H	OCH_3	OCH_3	OCH_3	H
3e	OCH_3	H	H	H	H
3f	OCH_3	OCH_3	OCH_3	H	H

Group 4

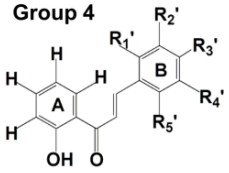

	R1'	R2'	R3'	R4'	R5'
4a	H	H	H	H	H
4b	OCH_3	H	H	H	H
4c	H	H	OCH_3	H	H
4d	OCH_3	H	OCH_3	H	H
4e	OCH_3	H	H	OCH_3	H
4f	OCH_3	OCH_3	OCH_3	H	H
4g	H	OCH_3	OCH_3	OCH_3	H
4h	OCH_3	H	OCH	OCH_3	H
4i	OCH_3	H	OCH_3	H	OCH_3
4j	OH	H	H	H	H
4k	H	OH	H	H	H
4l	H	H	OH	H	H
4m	H	H	H	OH	H
4n	OCH_3	H	H	H	OH

	R1'	R2'	R3'	R4'	R5'
4o	H	H	OCH_3	OH	H
4p	H	H	F	H	H
4q	H	H	Cl	H	H
4r	Cl	H	Cl	H	H
4s	Cl	H	H	H	Cl
4t	H	Cl	Cl	H	H
4u	H	H	Br	H	H
4v	H	H	$C(CH_3)_3$	H	H
4w	H	H	$(CH_3CH_2)_2NH$	H	H
4x	H	H	CH_2CH_3	H	H
4y	H	H	$(CH_3)_2CHCH_2$	H	H
4z	H	H	C_4H_9	H	H
4aa	H	H	C_3H_5	H	H

Group 5

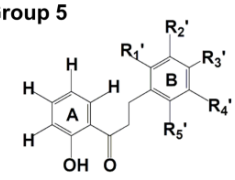

	R1'	R2'	R3'	R4'	R5'
5a	H	H	OH	H	H

Group 6

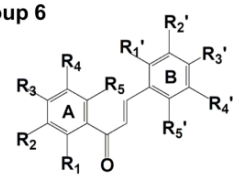

	R1	R2	R3	R4	R5	R1'	R2'	R3'	R4'	R5'
6a	H	H	OH	H	OH	H	H	OH	H	H
6b	OH	H	H	H	OCH_3	H	H	OCH_3	H	H
6c	OH	Br	H	Br	H	H	H	OH	H	H
6d	OH	H	OCH_3	H	OH	H	H	H	H	H
6e	OH	H	OH	H	H	H	H	OCH_3	H	H
6f	OCH_3	H	OH	H	OH	H	H	H	H	H

Figure 2. Chemical structures of the three known compounds 1335528, 2122620, and 4-hydroxyderricin as well as the 47 designed chalcones in six groups.

EBNA1 protein were added with help of the LEaP module. The antechamber and parmchk modules were used to generate restrained electrostatic potential charges of chalcones. The AMBER ff14SB and GAFF force field parameters were taken for both the protein and the ligands, respectively (Mahalapbutr *et al.*, 2017). The complex geometries with the added hydrogen atoms were then minimized with 1000 steps of the steepest descents (SD) approaches and subsequently by 3000 steps of conjugated gradient (CG) approaches. Afterwards, solvation of each system was performed by TIP3P (Wang, Wolf, Caldwell, Kollman, & Case, 2004) water molecules of approximately 14,810 atoms in a periodic box at a distance of 12 Å apart from the protein surface. The dimensions of the box used for all simulations were 84×84×85 Å. A periodic boundary condition with NPT ensemble and a step-size of 2 fs for the simulation time were used. The water molecules were then only minimized with 1000 steps of SD and continued by 3000 steps of CG. Positive charges of complexes were randomly neutralized by Cl^- counter ions. In the last step, all systems were fully minimized by the same minimization process. All bonds with hydrogen atoms were constrained using the SHAKE algorithm (Jorgensen, Chandrasekhar, Madura, Impey, & Klein, 1983). The MD simulations were performed until 100 ns. The solvent accessible surface area (SASA) and the root mean square displacement (RMSD) as well as the hydrogen bond occupation were calculated using the cpptraj module. MM/GBSA binding free energies and the per-residue decomposition energies were estimated by the MMGBSA.py module of AMBER16.

2.3 Calculation of the binding free energy

The MM/GBSA-based binding free energy calculations (Ryckaert, Ciccotti, & Berendsen, 1977) were conducted using the 100 MD snapshots from the last 20 ns of the simulation. In this method, binding free energies (ΔG_{bind}) between EBNA1 and the respective ligand were calculated by computing the free energy difference between the ligand-EBNA1 complex ($\Delta G_{complex}$) and the distinctive forms (ΔG_{EBNA1} and ΔG_{ligand}) as depicted in Equation 1:

$$\Delta G_{bind} = \Delta G_{complex} - (\Delta G_{EBNA1} + \Delta G_{ligand}) \quad (1)$$

where $\Delta G_{complex}$, ΔG_{EBNA1}, and ΔG_{ligand} are the free energies of the complex, EBNA1, and the ligand, respectively. The total free energy of a given conformation (state i) contains the enthalpy and entropy contributions expressed by Equation 2:

$$\Delta G_i = \Delta H_i - T\Delta S_i \quad (2)$$

where ΔH is the sum of the enthalpy changes in the gas phase upon complex formation (ΔE_{MM}), and the solvation free energy contribution (ΔG_{solv}). $-T\Delta S$ is the entropy contribution to the binding process. Therefore, Equation 2 can be modified giving Equation 3:

$$\Delta G_{bind} = \Delta E(_{MM})_i + \Delta G(_{solv})_i - T\Delta S \quad (3)$$

where the free energy (ΔG_{bind}) is the sum of the molecular mechanical energy in the gas phase (ΔE_{MM}), the solvation free energy (ΔG_{solv}), and the entropy term (ΔS). The free energy (ΔG_{bind} = complex, protein, and ligand) can be computed using the MM/GBSA method. The ΔE_{MM} is obtained by combining electrostatic (ΔE_{ele}) and van der Waals (ΔE_{vdW}) energies between ligand and its receptor using Equation 4.

$$\Delta E_{MM} = \Delta E_{ele} + \Delta E_{vdW} \quad (4)$$

The ΔG_{solv} can be separated into the electrostatic ($\mathbf{\Delta G^{ele}_{solv}}$) and the non-electrostatic solvation energy ($\mathbf{\Delta G^{ele}_{nonpolar}}$) as given in Equation 5.

$$\Delta G_{solv} = \mathbf{\Delta G^{ele}_{solv}} + \mathbf{\Delta G^{ele}_{nonpolar}} \quad (5)$$

The electrostatic solvation energy (polar component) is calculated with the help of the generalized Born model (Hou, Wang, Li, & Wang, 2011). The dielectric constants for the solute as well as for the surrounding solvent were set to 1 and 80, respectively (Mongan, Simmerling, McCammon, Case, & Onufriev, 2007). The non-polar contribution (the non-electrostatic solvation energy) is approximated by the scheme given in Equation 6:

$$\mathbf{\Delta G^{ele}_{nonpolar}} = \gamma * SASA + b \quad (6)$$

where γ is equal to 0.00542 kcal/mol·$A^{\circ 2}$, and b is equal to 0.92 kcal/mol (Izadi, Aguilar, & Onufriev, 2015). The SASA is defined by a radius of 1.4 Å for the probe molecule. The entropy of the solute is approximated by a normal mode analysis (Sitkoff, Sharp, & Honig, 1994). Moreover, the contribution of each amino acid for ligand binding was determined using the per-residue decomposition free energy ($\mathbf{\Delta G^{residue}_{bind}}$) based on the MM/GBSA method.

3. Results and Discussion

3.1 Molecular docking study

To screen the 47 designed chalcones, each compound was docked into the RH site using both CDOCKER and iGEMDOCK (Figure 3). The docking results from the two different methods showed the same trend. Chalcones 3a, 3b, and 3d contained a hydroxyl group at the ortho position and two methoxyl groups at the ortho and para positions on ring A, while chalcones 4g and 4h had a hydroxyl group at the ortho position. All chalcones exhibited lower interaction energies than the others as well as lower or equal interaction energies to those of the three known compounds used as reference compounds (1335528, 2122620, and 4-hydroxyderricin) (Akihisa *et al.*, 2003; Gianti, Messick, Lieberman, & Zauhar, 2016). This finding suggested that these chalcones could be potent candidates acting against the EBNA1 target. Thus, the five chalcones were then selected to investigate the dynamic behaviors and ligand-target binding interactions in an aqueous solution as well as to predict the inhibitory activity using MD simulations and MM/GBSA binding free energy calculations in comparison with three known inhibitors.

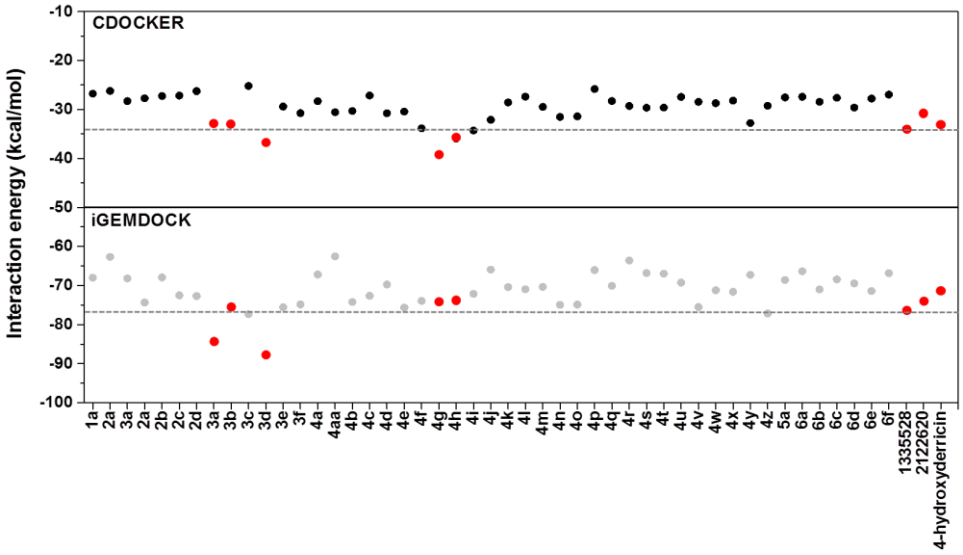

Figure 3. Interaction energies (kcal/mol) from CDOCKER (top) and iGEMDOCK (bottom) of 47 chalcones and 3 known inhibitors (1335528, 2122620, and 4-hydroxyderricin) in complex with EBNA1.

3.2 Stability of the simulated models

The stability of all simulated ligand-EBNA1 complexes was visualized by RMSD and compared with the starting structure as depicted in Figure 4. The RMSD values of all complexes (black) were maintained at a fluctuation of ~6.0–6.3 Å until the end of simulation time (except for the 4h system). Note that the 3d and 4h compounds moved out of the RH site even though the other two simulations with different velocities were performed. This suggests that these two compounds are likely unstable and may not bind with EBNA1 in solution. The RMSD pattern of protein EBNA1 (light grey) and backbone of protein EBNA1 (dark grey) was similar for all systems (except for the 4h system), while the RMSDs of ligand (grey) showed a low fluctuation compared to its initial structure. In this study, the last 20 ns of MD trajectories of chalcones systems were extracted for further analysis for comparison with the 1335528, 2122620, and 4-hydroxyderricin systems.

3.3 Binding free energy prediction for ligand-EBNA1 complex

The MM/GBSA based binding free energies for EBNA1 with eight ligands were calculated from the last 20 ns using 100 snapshots (Table 1). As expected, due to the hydrophobicity of all compounds, vdW interaction was the main force inducing ligand-EBNA1 binding. Interestingly, the averaged binding free energies of chalcones 3a (–9.3±0.8 kcal/mol) and 3b (–7.0±0.8 kcal/mol) are significantly lower than those of the known active compounds 1335528 (–6.8±1.1 kcal/mol), 2122620 (–5.2±1.1 kcal/mol), and 4-hydroxyderricin (–4.1±0.8 kcal/mol) which suggested that these two chalcones could potentially inhibit EBNA1. Notably, our MM/GBSA approaches were able to predict the binding free energy values of the two inhibitors 1335528 and 2122620 against EBNA1 somewhat close to the experimental data (ΔG_{exp} of −7.1 kcal/mol and −6.3 kcal/mol). Note that, the ΔG_{exp} was obtained from the IC_{50} values of 6.659 μM and 26.951 μM where IC_{50} was the drug concentration which inhibited the enzyme activity by 50%. In addition, the binding free energies of chalcones 3d (0.4±0.9 kcal/mol) and 4h (2.5±1.3 kcal/mol) confirmed that compounds 3d and 4h did not preferably interact with EBNA1 and moved out of the RH site. Only the 3a, 3b, and 4g systems were then analyzed further.

3.4 Binding pattern of screened chalcones

In order to investigate the key residues which are involved in ligand binding within the RH site, the per-residue

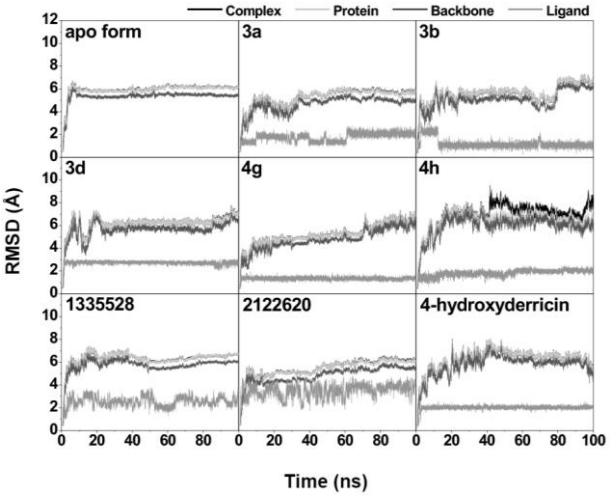

Figure 4. Root mean square displacement (RMSD) plot for all atoms (black), protein (light grey), backbone atoms (dark grey), and ligand atoms (grey) for all studied ligand-EBNA1 complexes.

decomposition free energy ($\Delta G_{bind}^{residue}$) calculations were performed by the MM/GBSA method. The same set of 100 snapshots was used as in the former session. The contribution of each amino acid for the ligand binding for all complexes is given in Figure 5a. The negative and positive decomposition free energy values are a measure of the ligand attraction and repulsion, respectively. Additionally, the binding orientations of 3a, 3b, 4g, 1335528, 2122620, and 4-hydroxyderricin inside the RH site are displayed in Figure 5b. The results showed that Pro476, Lys477, Asn480, Ile481, Asn519, Leu582, Lys586, and Thr590 were found to be the key binding residues for ligand binding. The findings corresponded with a previous study (Gianti, Messick, Lieberman, & Zauhar, 2016) in which Lys477, Asn480, Asn519, and Lys586 were found to be the important residues in establishing interactions with compounds 1335528 and 2122620.

Hydrogen bonding is an important factor in ligand-target interactions. Consequently, the percentage of intermolecular hydrogen bonding was determined according to two criteria: (i) distance between the hydrogen donor (HD) and hydrogen acceptor (HA) lower than 3.5 Å and (ii) the angle of HD–H···HA more than 120°. Schematic views of hydrogen bonding formed between each ligand and its binding residues extracted from the last snapshot are given in Figure. 6. The important residues contributed to ligand stabilization through a firmed hydrogen bond formation are likely from Asn475 for 4g, Asn480 for 1335528, Asn519 for 3a, 3b, and 1335528, and Leu582 for 2122620. These intermolecular hydrogen bonds somewhat support the ligand binding to EBNA1, but is not the main force for ligand-target complexation as discussed above in terms of molecular mechanics energy (Table 1).

3.5 Solvent accessibility at the RH site

The SASA calculation of the protein residues within a 5 Å sphere of ligand (residues 464-471, 475-488, 513-520, and 579-590) was performed to investigate the effect of solvent accessibility on the RH site. The results are summarized and compared in Figure 7. The SASA value over the last 20 ns of the RH site without ligand binding (apo form)

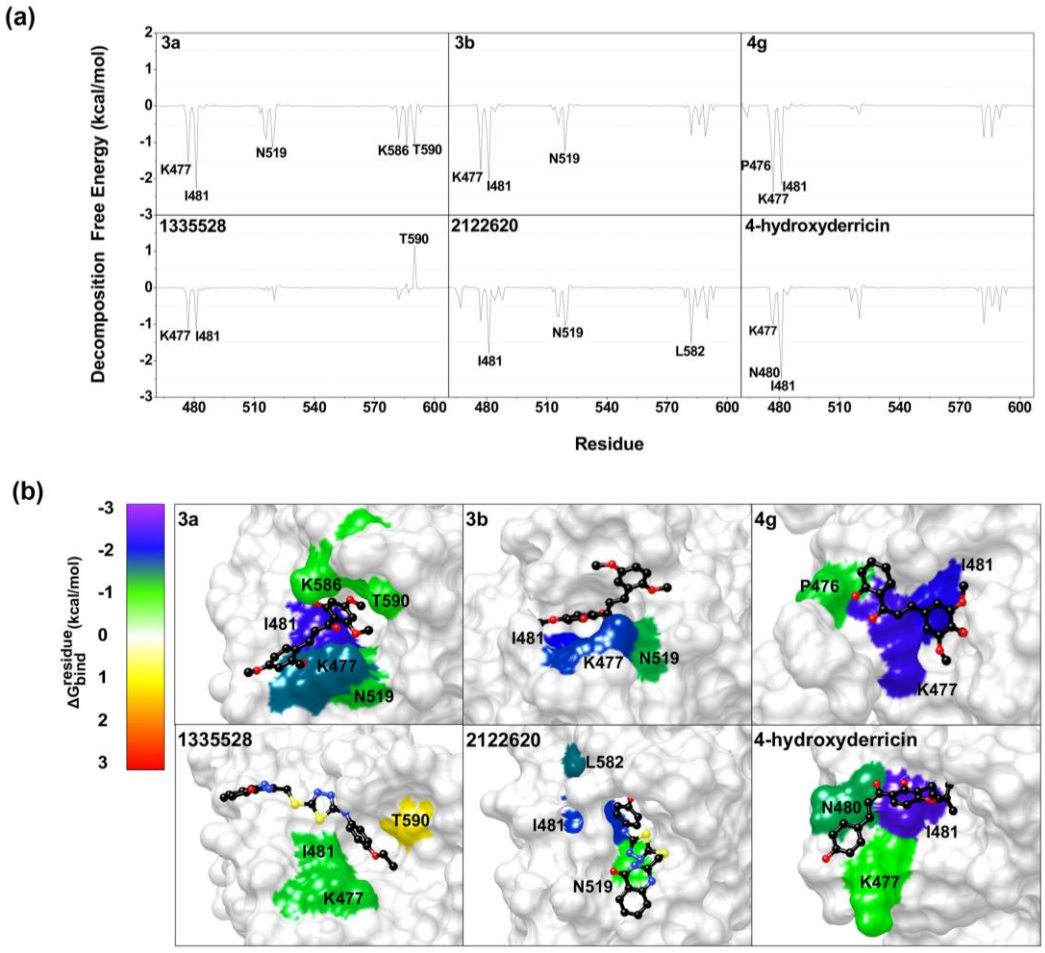

Figure 5. (a) Per-residue decomposition free energy ($\Delta G_{bind}^{residue}$) of the EBNA1 protein for the binding of 3a, 3b, 4g, 1335528, 2122620, and 4-hydroxyderricin, (b) Binding orientation inside the recognition helix site drawn from the last MD snapshot. The EBNA1 residues involved in ligand binding are shaded according to their $\Delta G_{bind}^{residue}$ values in which the lowest and highest energies range from purple (−3 kcal/mol) to red (3 kcal/mol), respectively.

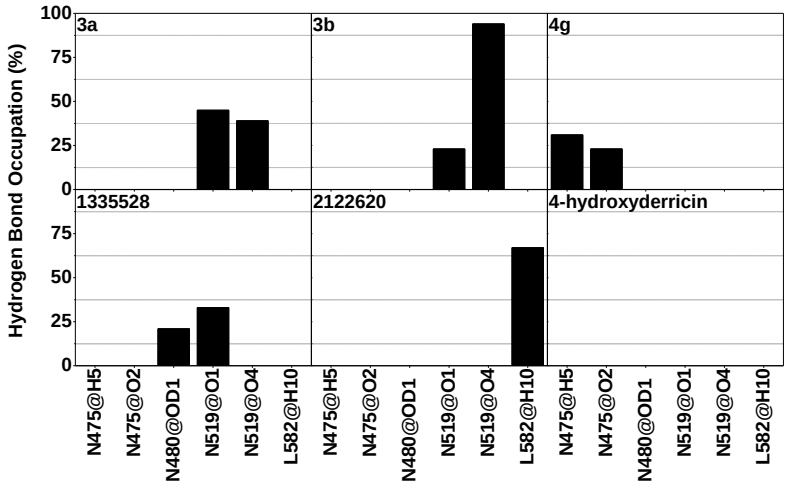

Figure 6. Percentages of hydrogen bonding for the six ligands with EBNA1 residues evaluated over the last 20 ns.

Table 1. MM/GBSA binding free energy and its energy components (kcal/mol) for 3a, 3b, 3d, 4g, 4h, 1335528, 2122620, and 4-hydroxyderricin in complex with EBNA1.

	3a	3b	3d	4g
ΔE_{vdw}	−34.62±0.28	−31.21±0.35	−26.63±0.47	−31.33±0.28
ΔE_{elec}	−17.15±0.57	−18.98±0.56	−9.23±0.63	−13.37±0.36
ΔE_{MM}	−51.77±0.68	−50.18±0.63	−35.87±0.93	−44.70±0.43
ΔG_{polar}	29.52±0.51	30.47±0.50	20.94±0.67	26.80±0.33
$\Delta G_{non\text{-}polar}$	−4.96±0.03	−4.59±0.05	−3.39±0.07	−4.45±0.03
ΔG_{sol}	24.57±0.50	24.22±0.35	17.55±0.62	22.35±0.32
$-T\Delta S$	17.93±1.19	17.26±1.35	17.99±1.21	0.56±0.87
ΔG_{bind}	−9.27±0.79	−7.04±0.78	0.36±0.92	−3.90±0.54
ΔG_{exp}	N/A	N/A	N/A	N/A
	4h	1335528	2122620	4-hydroxyderricin
ΔE_{vdw}	−18.47±0.79	−31.53±0.29	−34.60±0.41	−31.11±0.26
ΔE_{elec}	−7.10±0.74	−20.19±1.01	−5.34±0.97	−0.51±0.56
ΔE_{MM}	−25.57±1.13	−55.72±1.06	−39.94±1.02	−31.62±0.59
ΔG_{polar}	16.46±0.85	30.52±0.85	25.15±0.89	14.20±0.51
$\Delta G_{non\text{-}polar}$	−2.48±0.10	−4.44±0.04	−5.29±0.04	−4.46±0.03
ΔG_{sol}	13.98±0.79	26.08±0.83	12.36±0.88	9.74±0.51
$-T\Delta S$	1.71±1.85	22.81±1.34	22.42±1.29	17.81±1.34
ΔG_{bind}	2.50±1.26	−6.84±1.08	−5.15±1.06	−4.07±0.81
ΔG_{exp}	N/A	−7.1	−6.3	N/A

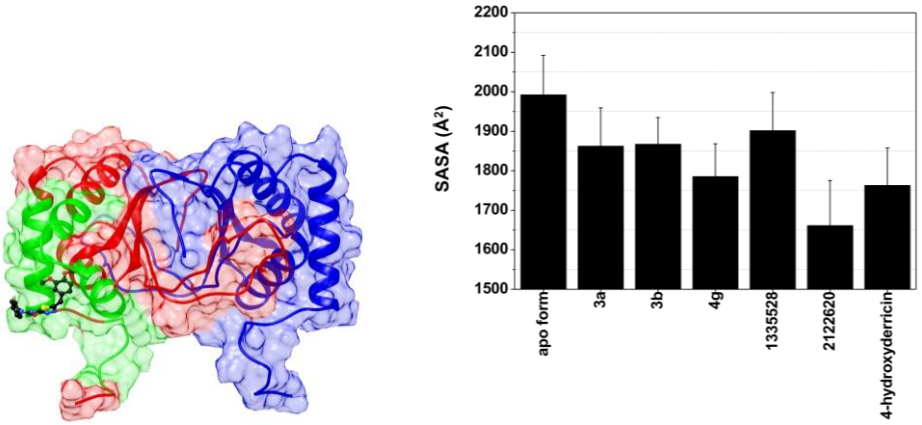

Figure 7. Solvent accessible surface area (SASA) within a 5 Å sphere of ligand in chain A (red) represented by green color.

of 1993±99 Å^2 was observed, which was higher than all ligand binding in chain A. This suggested that the focused chalcones, i.e. 3a, 3b, and 4g, fit well within the RH site as also found for the known inhibitors.

4. Conclusions

In the present study, 47 designed derivatives of chalcone were used for anti-EBV drug screening using computational approaches. Molecular docking based on CDOCKER and iGEMDOCK techniques suggested that chalcones 3a, 3b, and 3d containing a hydroxyl group at the ortho position and two methoxyl groups at the ortho and para positions on ring A and the chalcones 4g and 4h containing a hydroxyl group at the ortho position on this ring preferentially bonded with the EBNA1 more than other compounds. Their interaction energies were also lower or equal to the known anti-EBV agents, 1335528, 2122620, and 4-hydroxyderricin and thus they were selected for the MD study. According to per residue decomposition free energy analysis, the amino acid residues Pro476, Lys477, Asn480, Ile481, Asn519, Leu582, Lys586, and Thr590 were found to be potent binding residues for ligands according to the residue decomposition free energy analysis. Van der Waals interactions were found to be higher than electrostatic interactions and hydrogen bonding. The MM/GBSA binding free energies showed that, among the focused compounds, 3a exhibited the greatest binding affinity. The theoretically obtained results give valuable information on the structures and dynamics of the complexes with regard to the binding orientation of ligands and the amino acid side chain residues of the ligand binding pocket. In summary, it is suggested that the screened chalcone 3a be tested further for the inhibitory activity toward EBNA1 for further use as a lead compound in anti-EBV drug design and development.

Acknowledgements

The financial support by the Research Chair Grant, the National Science and Technology Development Agency (NSTDA), Thailand it gratefully acknowledged. N.D. would like to thank the Thailand Graduate Institute of Science and Technology (TGIST Grant No. TG550959036M). N.K. wants to thank the Research Center on Chemistry for Development of Health Promoting Products from Northern Resources, Chiang Mai University. Thanks should be given to the Structural and Computational Biology Research Group, Special Task Force for Activating Research (STAR), Faculty of Science, Chulalongkorn University as well as to the Thailand Research Fund (IRG5780008). We thank Prof. Apiwat Mutirangura and Assoc. Prof. Warinthorn Chavasiri for providing the research topic and for fruitful discussions. This work was also supported by ASEA-UNINET. The Computational Chemistry Center of Excellence, and the Vienna Scientific Cluster (VSC-2) should be mentioned for generously providing the computer facilities and computing resources.

References

Akihisa, T., Tokuda, H., Ukiya, M., Iizuka, M., Schneider, S., Ogasawara, K., & Nishino, H. (2003). Chalcones, coumarins, and flavanones from the exudate of Angelica keiskei and their chemopreventive effects. *Cancer Letters, 201*, 133-137. Retrieved from https://www.ncbi.nlm.nih.gov/pubmed/14607326

Bernini, R., Mincione, E., Coratti, A., Fabrizi, G., & Battistuzzi, G. (2004). Epoxidation of chromones and flavonoids in ionic liquids. *Tetrahedron, 60*, 967-971. doi:10.1016/j.tet.2003.11.032

Bochkarev, A., Bochkareva, E., Frappier, L., & Edwards, A. M. (1998). The 2.2 Å structure of a permanganate-sensitive DNA site bound by the Epstein-Barr virus origin binding protein, EBNA1. *Journal of Molecular Biology, 284*, 1273-8. doi:10.1006/jmbi.1998.2247

Boudreault, S., Armero, V., Scott, M. S., Perreault, J. P., & Bisaillon, M. (2019). The Epstein-Barr virus EBNA1 protein modulates the alternative splicing of cellular genes. *Virology Journal, 16*, 2019. doi:10.1186/s12985-019-1137-5

Choudhary, A. L., & Juyal, V. (2011). Synthesis of chalcone and their derivatives as antimicrobial agents. *International Journal of Pharmacy and Pharmaceutical Sciences, 3*, 125-128. Retrieved from https://innovareacademics.in/journal/ijpps/Vol3Issue3/2208.pdf

Cohen, J. I. (2000). Epstein-Barr virus infection. *The New England Journal of Medicine, 343*, 481-92. doi:10.1056/NEJM200008173430707.

Evranos, A. B., & Ertan, R. (2011). Chemical and structural properties of chalcones I. *Journal of Pharmaceutical Sciences, 36*, 223-242. Retrieved from https://www.academia.edu/27645205

Frisch, M., Trucks, G. W., Schlegel, H. B., Scuseria, G. E., Robb, M. A., & Cheeseman, J. R. (2009). *Gaussian 09*. Wallingford, CT: Gaussian.

Gianti, E., Messick, T. E., Lieberman, P. M., & Zauhar, R. J. (2016). Computational analysis of EBNA1 "drug gability" suggests novel insights for Epstein-Barr virus inhibitor design. *Journal of Computer-Aided Molecular Design, 30*, 285-303. doi:10.1007/s10822-016-9899-y

Hou, T., Wang, J., Li, Y., & Wang, W. (2011). Assessing the performance of the MM/PBSA and MM/GBSA methods: I. The accuracy of binding free energy calculations based on molecular dynamics simulations. Journal of chemical information and modeling. *Model, 51*, 69-82. doi:10.1021/ci100275a

Izadi, S., Aguilar, B., & Onufriev, A. V. (2015). Protein-ligand electrostatic binding free energies from explicit and implicit solvation. *Journal of chemical theory and computation, 11*, 4450-4459. doi:10.1021/acs.jctc.5b00483

Jinn-Moon, Y., & Chun-Chen, C. (2004). GEMDOCK: A Generic Evolutionary Method for Molecular Docking. *PROTEINS: Structure, Function, and Bioinformatics, 55*, 288–304. doi:10.1002/jcc.10306

Jorgensen, W. L., Chandrasekhar, J., Madura, J. D., Impey, R. W., & Klein, M. L. (1983). Comparison of simple potential functions for simulating liquid water. *The Journal of chemical physics, 79*, 926-935. doi:10.1063/1.445869

Leight, E. R., & Sugden, B. (2000). EBNA-1: A protein pivotal to latent infection by Epstein-Barr virus. *Reviews in Medical Virology, 10*, 83-100. Retrieved from https://www.ncbi.nlm.nih.gov/pubmed/10713596

Li, N., Thompson, S., Schultz, D. C., Zhu, W., Jiang, H., Luo, C., & Lieberman, P. M. (2010). Discovery of selective inhibitors against EBNA1 via high throughput in silico virtual screening. *PLoS One, 5*, e10126. doi:10.1371/journal.pone.0010126

Mahalapbutr, P., Chusuth, P., Kungwan, N., Chavasiri, W., Wolschann, P., & Rungrotmongkol, T. (2017). Molecular recognition of naphthoquinone-containing compounds against human DNA topoisomerase IIa ATPase domain: A molecular modeling study. *Journal of Molecular Liquids, 247*, 374-385. doi:10.1016/j.molliq.2017.10.021

Middeldorp, J. M. (2015). Epstein-barr virus-specific humoral immune responses in health and disease. *Epstein Barr Virus, 2*, 289-323. doi:10.1007/978-3-319-22834-1_10

Mongan, J., Simmerling, C., McCammon, J. A., Case, D. A., & Onufriev, A. (2007). Generalized born model with a simple, robust molecular volume correction. *Journal of Chemical Theory and Computation, 3*, 156-169. doi:10.1021/ct600085e

Nutho, B., Khuntawee, W., Rungnim, C., Pongsawasdi, P., Wolschann, P., Karpfen, A., & Rungrotmongkol, T. (2014). Binding mode and free energy prediction of fisetin/beta-cyclodextrin inclusion complexes. *The Journal of Organic Chemistry, 10*, 2789-2799. doi:10.3762/bjoc.10.296

Olsson, M. H. M., Sondergaard, C. R., Rostkowski, M., & Jensen, J. H. (2011). Consistent treatment of internal and surface residues in empirical pKa predictions. *Journal of Chemical Theory and Computation, 7*, 525-537. doi:10.1021/ct100578z

Ryckaert, J. P., Ciccotti, G., & Berendsen, H. J. C. (1977). Numerical integration of the cartesian equations of motion of a system with constraints: Molecular dynamics of n-alkanes. *Journal of Computational Physics, 23*, 327-341. doi:10.1016/0021-9991(77)90098-5

Sangpheak, W., Khuntawee, W., Wolschann, P., Pongsawasdi, P., & Rungrotmongkol, T. (2014). Enhanced stability of a naringenin/2, 6-dimethyl beta-cyclodextrin inclusion complex: molecular dynamics and free energy calculations based on MM- and QM-PBSA/GBSA. *Journal of Molecular Graphics and Modelling, 50*, 10-15. doi:10.1016/j.jmgm.2014.03.001

Schepers, A., Ritzi, M., Bousset, K., Kremmer, E., Yates, J. L., Harwood, J., & Hammerschmidt, W. (2001). Human origin recognition complex binds to the region of the latent origin of DNA replication of Epstein-Barr virus. *The EMBO Journal, 20*, 588-602. doi:10.1093/emboj/20.16.4588

Sitkoff, D., Sharp, K. A., & Honig, B. (1994). Accurate calculation of hydration free energies using macroscopic solvent models. *The Journal of Physical Chemistry, 98*, 1978-1988. doi:10.1021/j100058a043

Vrzalikova, K., Sunmonu, T., Reynolds, G., & Murray, P. (2018). Contribution of Epstein–Barr virus latent proteins to the pathogenesis of classical hodgkin lymphoma. *Pathogens, 3*, 59. doi:10.3390/pathogens7030059

Wang, J., Wolf, R. M., Caldwell, J. W., Kollman, P. A., & Case, D. A. (2004). Development and testing of a general amber force field. *Journal of Computational Chemistry, 25*, 1157-1174. doi:10.1002/jcc.20035

Wu, G., Robertson, D. H., Brooks, C. L., & Vieth, M. (2003). Detailed analysis of grid-based molecular docking: A case study of CDOCKER-A CHARMm-based MD docking algorithm. *Journal of Computational Chemistry, 24*, 1549-1562. doi:10.1002/jcc.10306

Yasuda, A., Noguchi, K., Minoshima, M., Kashiwazaki, G., Kanda, T., Katayama, K., & Sugimoto, Y. (2011). DNA ligand designed to antagonize EBNA1 represses Epstein-Barr virus-induced immortalization. *Cancer Science, 102*, 2221-2230. doi:10.1111/j.1349-7006.2011.02098.x